

Design and Application for PV Generation System Using a Soft-Switching Boost Converter with SARC

T.Venugopal¹, B.Bhavsingh²

^{1,2}Electrical and Electronics Engineering Department, Vaagdevi college of Engineering, Warangal

Abstract—In order to improve the efficiency of energy conversion for a photovoltaic (PV) system, a soft-switching boost converter using a simple auxiliary resonant circuit, which is composed of an auxiliary switch, a diode, a resonant inductor, and a resonant capacitor, is adopted in this paper. The conventional boost converter decreases the efficiency because of hard switching, which generates losses when the switches are turned on/off. During this interval, all switches in the adopted circuit perform zero-current switching by the resonant inductor at turn-on, and zero-voltage switching by the resonant capacitor at turn-off. This switching pattern can reduce the switching losses, voltage and current stress of the switching device. Moreover, it is very easy to control. In this paper, we have analyzed the operational principles of the adopted soft-switching boost converter, and it is designed for PV generation system. Simulation and experimental results are presented to confirm the theoretical analysis.

Index Terms—Auxiliary resonant circuit, photovoltaic (PV), soft-switching boost converter, zero-current switching (ZCS), zero-voltage switching (ZVS).

NOMENCLATURE

i_{S1} Main switch current.
 i_{S2} Auxiliary switch current.
 i_L Main inductor current.
 i_{Lr} Resonant inductor current.
 I_{min} Minimum current of the main inductor.
 I_{max} Maximum current of the main inductor.
 $I_{Lr, max}$ Maximum current of the resonant inductor.
 Δi_L Current ripple of the main inductor.
 $V_{S, min}$ Minimum output voltage of the solar cell.
 $V_{S, max}$ Maximum output voltage of the solar cell.
 v_L Main inductor voltage.
 v_{Lr} Resonant inductor voltage.
 v_{Cr} Resonant capacitor voltage.
VFW Freewheeling voltage drop at mode 4.
 D_{eff} Effective duty ratio.

I. INTRODUCTION

Before increased research about renewable energy, most of the energy used in industry depended on fossil fuel. But these days, because of fuel fossil exhaustion, which is due to limited reserves and environmental problems, the development and demand for renewable energy has increased. Fuel cells, water, wind, and photovoltaic (PV) energy are all renewable energy sources. Of these, PV energy is limitless and clean. The solar cell has nonlinear $V-I$ and $P-V$ characteristics, which depend on the irradiance, the operating temperature and load condition of the cell. Therefore, the dc-dc converter for a PV system has to control the variation of the maximum power point of the solar cell output. In other words, modulation of the duty ratio of the dc-dc converter controls maximum power point tracking (MPPT) [1], [2].

Recently, switch-mode power supplies have become smaller and lighter, because the switching frequency has increased. However, as the switching frequency has increased, the periodic losses at turn-on/off have also increased. As a result, this loss brings increasing loss of whole system. Therefore, to reduce these switching losses, a soft-switching method is proposed, which involves an added auxiliary circuit, instead of a conventional hard-switching converter [3]–[12]. However, the auxiliary circuit for resonance increases the complexity and cost. For some resonant converter with auxiliary switch, main switch achieves soft-switching but auxiliary switch performs hard switching. Thus, these converters cannot improve the whole system efficiency owing to switching loss of auxiliary switch.

This paper proposes the soft-switching boost converter applied to an auxiliary resonant circuit for a PV generation system. It has better efficiency than a conventional boost converter. Moreover, this converter boosts the lower output voltage of the solar cell to the useful voltage for the load. The adopted converter has a simple auxiliary resonant circuit (SARC). Through this circuit, all of the switching devices perform soft-switching under zero-voltage and zero-current conditions. Therefore, the periodic losses generated at turn-on and turn-off can be decreased. The adopted soft-switching boost converter

is designed for a 700 W PV module. In this paper, the adopted softswitching boost converter is simulated by Powersim (PSIM) software. Furthermore, its performance is confirmed by the PV simulator and experimental setup.

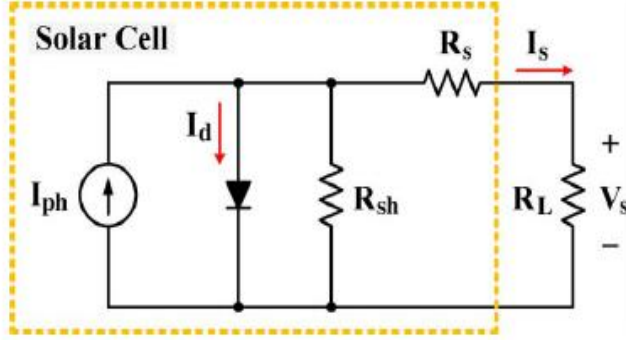


Fig. 1. Equivalent circuit of a solar cell.

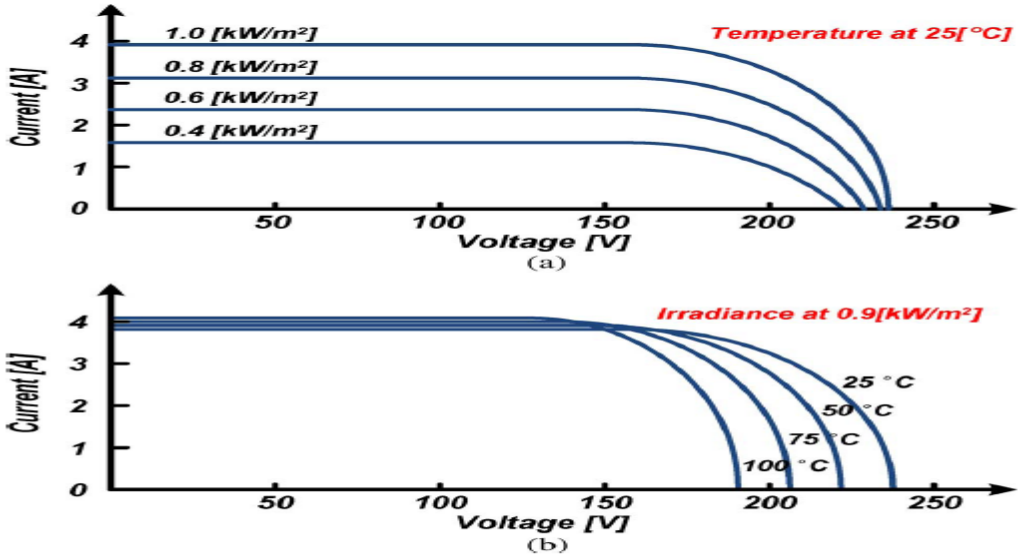


Fig. 2. Simulated $I-V$ characteristic curves of Solarsim-10k. (a) $I-V$ curves of the Solarsim-10k PV simulator influenced by different irradiances when the operating temperature is constant at 25 °C. (b) $I-V$ curves of the Solarsim-10k PV simulator influenced by different operating temperatures when the irradiance is constant at 0.9 kW/m².

II. CHARACTERISTICS OF SOLAR CELL AND MODULE

A solar cell is a kind of p-n junction semiconductor device. It converts light energy into electrical energy. Generally, as shown in Fig. 1, the equivalent circuit of the solar cell is composed of the internal serial resistance (R_s) and the shunt resistance (R_{sh}) of the diode. The output characteristics of the solar cell depend on the irradiance and the operating temperature of the cell. The solar cell output characteristics are expressed as [2], [13]

$$I_s = I_{ph} - I_{sat} \left[\exp\left(\frac{q(V_s + I_s R_s)}{AKT}\right) - 1 \right] - \frac{V_s + I_s R_s}{R_{sh}}. \quad (1)$$

In (1), it is assumed that R_s equals zero and that R_{sh} equals infinity; thus, the equation can be simplified as

$$I_s = I_{ph} - I_{sat} \left[\exp\left(\frac{qV_s}{AKT}\right) - 1 \right]. \quad (2)$$

Irradiance and operating temperature are important factors influencing the solar cell characteristics. Fig. 2 shows the I - V curves of the PV module. If irradiance increases, the fluctuation of the open-circuit voltage is very little. However, the short circuit current has sharp fluctuations with respect to irradiance. However, for a rising operating temperature, the variation of the short-circuit current is decreased, and the open-circuit voltage is decreased in a nonlinear fashion [1]. As shown in Fig. 2, the output-voltage range of the PV module varies. Owing to this characteristic, the adopted converter must be designed for soft switching based on the output-voltage range of the PV module.

III. SOFT-SWITCHING BOOST CONVERTER FOR PV GENERATION SYSTEM

In Fig. 3, the adopted converter is controlled by ATmega128, which is an 8-bit microprocessor used to implement an MPPT [perturb and observe (P&O)]. Moreover, the PV simulator Solarsim-10K supplies the energy to this converter. The auxiliary circuit is composed of an auxiliary switch (S_2), a resonant capacitor (C_r), a resonant inductor (L_r), and twodiodes (D_1 and D_2) [14], [15].

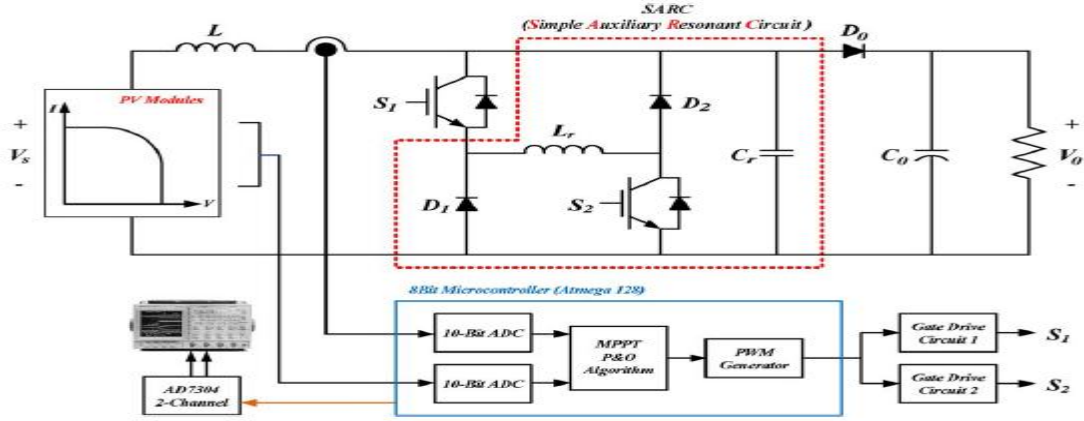


Fig. 3. Block diagram of the soft-switching boost converter.

Shown in Fig. 4, the operational principle of this converter can be divided into six intervals. For a simple analysis of each interval of this converter, the following assumptions are made.

- 1) All switching devices and passive elements are ideal.
- 2) The parasitic components of all switching devices and elements are negligible.
- 3) The input voltage (V_s) is in the range of 150–230 V.
- 4) This converter operates the continuous conduction mode at all intervals.

A. Interval 1 ($t_0 \leq t < t_1$)

Switches S_1 and S_2 are both in the OFF state, the current cannot flow through switches S_1 and S_2 , and the accumulated energy of the main inductor is transferred to the load (Fig. 5). In this interval, the main inductor current decreases linearly. During this time, the current does not flow to the resonant inductor, and the resonant capacitor has charged as output voltage. After two of the switches have been turned on, interval 1 is over. These conditions are as follows:

$$v_L(t) = V_s - V_o \quad (3)$$

$$i_L(t) = i_L(t_0) - \frac{V_o - V_s}{L} t \quad (4)$$

$$i_{D_o}(t) = i_L(t) \quad (5)$$

$$i_{L_r}(t) = 0 \quad (6)$$

$$v_{C_r}(t) = V_o. \quad (7)$$

B. Interval 2 ($t_1 \leq t < t_2$)

After turning on switches S_1 and S_2 , the current flows to the resonant inductor. At that time, two of the switches are turned on under zero-current condition. This is known as zero-current switching (ZCS). Because the main and auxiliary switches implement ZCS, this converter has lower switch loss than the conventional hard switching converter. As the

resonant current rises linearly, the load current gradually decreases. At t_2 , the main inductor current equals the resonant inductor current, and the output diode current is zero. When the resonant capacitor voltage equals V_o , the output diode is turned off, and interval 2 is over

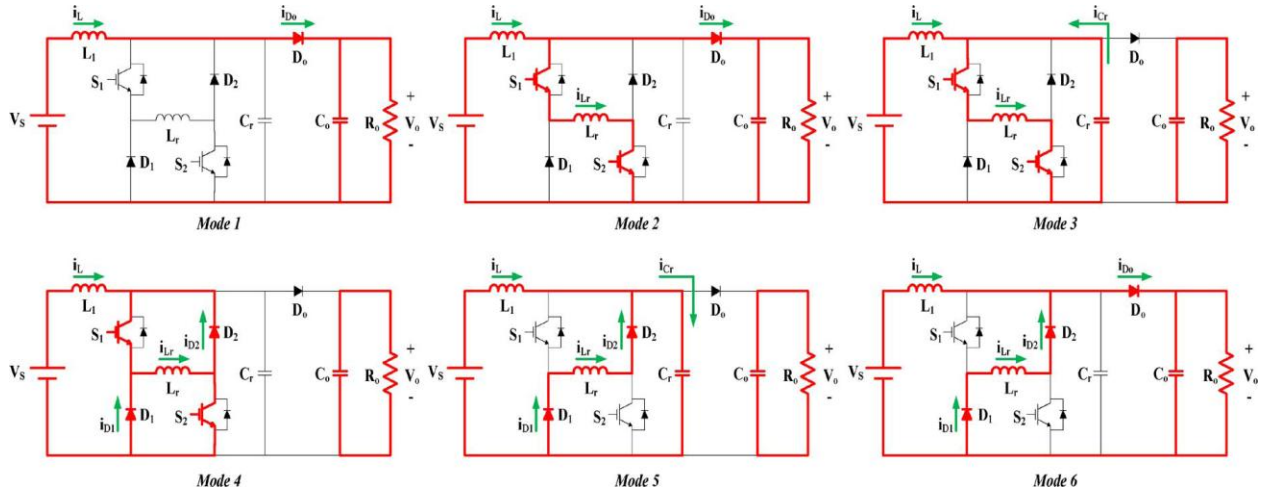


Fig. 4. Operational modes of the soft-switching boost converter for the PV generation system.

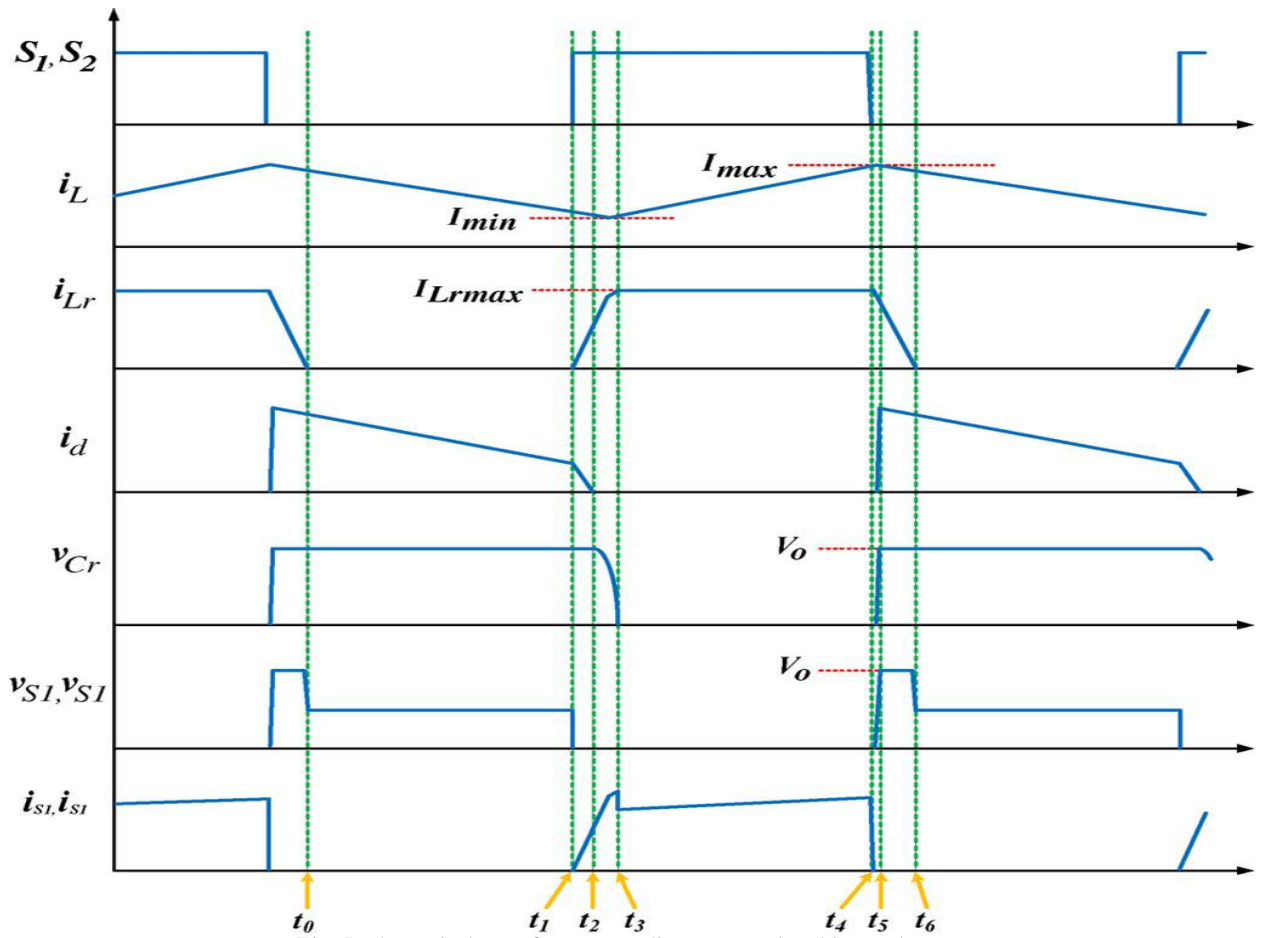


Fig. 5. Theoretical waveforms according to operational intervals.

$$i_{L_r}(t_1) = 0 \quad v_{L_r}(t) = V_o \quad (8)$$

$$i_{L_r}(t) = \frac{V_o}{L_r} t \quad (9)$$

$$i_L(t) = i_L(t_1) - \frac{V_o - V_s}{L} t \quad (10)$$

$$i_L(t_2) = i_{L_r}(t_2) \quad (11)$$

$$i_{D_o}(t_2) = 0. \quad (12)$$

C. Interval 3 ($t_2 \leq t < t_3$)

The current that flowed to the load through output diode D_o no longer flows, since t_2 and the resonant capacitor C_r , and the resonant inductor L_r start a resonance. The current flowing to the resonant inductor is a combination of the main inductor current and the resonant capacitor current. The amount of resonant current is expressed as (14)

$$i_L(t) \cong I_{\min} \quad (13)$$

$$i_{L_r}(t) = I_{\min} + \frac{V_o}{Z_r} \sin \omega_r t. \quad (14)$$

During this resonant period, the resonant capacitor C_r is discharged from V_o to zero. This is expressed as (15). Resonant frequency and impedance are given by (16) and (17). When the voltage of the resonant capacitor equals zero, the interval 3 is over

$$v_{C_r}(t) = V_o \cos \omega_r t \quad (15)$$

$$v_{C_r}(t_2) = V_o \quad v_{C_r}(t_3) = 0 \quad (16)$$

$$\omega_r = \frac{1}{\sqrt{L_r C_r}} \quad Z_r = \sqrt{\frac{L_r}{C_r}}. \quad (17)$$

D. Interval 4 ($t_3 \leq t < t_4$)

After the resonant period in interval 3, when the voltage of the resonant capacitor equals zero, interval 4 begins. In this interval, the freewheeling diodes of D_1 and D_2 are turned on, and the current of the resonant inductor is the maximum value. The resonant inductor current flows to the freewheeling diodes $S_1-L_r-D_2$ and $S_2-L_r-D_1$ along the freewheeling

$$i_{L_r}(t) = i_L(t) + i_{D_1}(t) + i_{D_2}(t) \quad (18)$$

$$i_{L_r}(t_3) = i_{L_r}(t_4) = I_{L_r, \max}. \quad (19)$$

path

During this time, the main inductor voltage equals the input voltage, and the current accumulating energy increases linearly

$$v_L(t) = V_s \quad (20)$$

$$i_L(t) = I_{\min} + \frac{V_s}{L} t. \quad (21)$$

E. Interval 5 ($t_4 \leq t < t_5$)

In interval 5, all of switches are turned off under the zero voltage condition by the resonant capacitor. During this interval, the initial conditions of the resonant inductor current and resonant capacitor voltage are as follows:

$$i_{L_r}(t_4) = I_{L_r, \max} \quad (22)$$

$$v_{C_r}(t_4) = 0. \quad (23)$$

When all of the switches are turned off, the resonant capacitor C_r is charged to the output voltage by two of the inductor currents. Until the resonant capacitor has been charged to V_o , the output diode is in the OFF state

$$i_L(t) \cong I_{\max} \quad (24)$$

$$i_{L_r}(t) = I_{\max} - (I_{\max} + I_{L_r, \max}) \cos \omega_r t \quad (25)$$

$$v_{C_r}(t) = Z_r (I_{\max} + I_{L_r, \max}) \sin \omega_r t \quad (26)$$

$$v_{C_r}(t_5) = V_o. \quad (27)$$

F. Interval 6 ($t_5 \leq t < t_6$)

Interval 6 begins when the resonant capacitor equals the output voltage, and the output diode is turned on under the zero-voltage condition. During this interval, the main inductor current i_L and the resonant inductor current i_{L_r} flow to the output through the output diode D_o

$$i_{D_o}(t) = i_L(t) + i_{L_r}(t) \quad (28)$$

$$i_{L_r}(t_5) = (I_{\max} + I_{L_r, \max}) \cos \omega_r (t_5 - t_4) - I_{\max} \quad (29)$$

$$v_{C_r}(t) = V_o. \quad (30)$$

At that time, two of the inductor currents are linearly decreased, and the energy of the resonant inductor is completely transferred to the load. Then, the interval 6 is over

$$i_L(t) = I_{\max} - \frac{V_o - V_s}{L_r} t \quad (31)$$

$$i_{L_r}(t) = i_{L_r}(t_6) - \frac{V_o}{L_r} t \quad (32)$$

$$i_{L_r}(t_6) = 0. \quad (33)$$

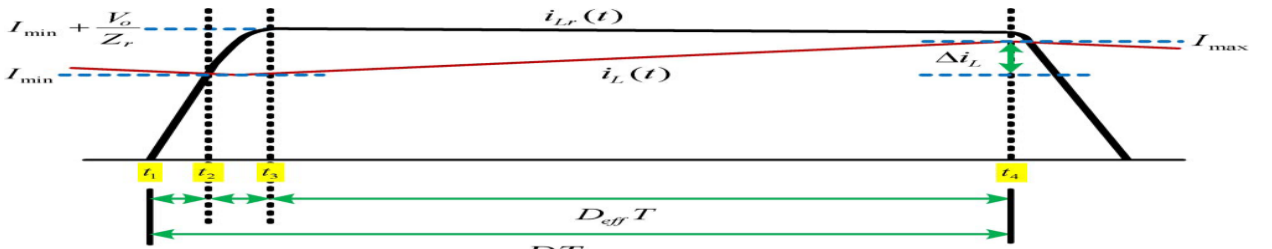


Fig. 6. ZVS condition.

IV. DESIGN PROCEDURE OF RESONANT INDUCTOR AND CAPACITOR IN SARC

A. ZVS Condition of Switch

Fig. 6 shows the key waveform of the soft-switching boost converter. To satisfy the zero-voltage switching (ZVS) condition, the resonant inductor current must exceed the main inductor current during the freewheeling interval of interval 4.

During interval 4, the voltage of the resonant inductor and the current are expressed by (36) and (37), respectively. The ZVS condition of this converter is expressed by (38)

$$D_{\min} = \frac{V_o - V_{s,\max}}{V_o} \quad (34)$$

$$D_{\max} = \frac{V_o - V_{s,\min}}{V_o} \quad (35)$$

$$v_{Lr}(t) = V_{ce, sat} + V_F = V_{FW} \quad (36)$$

$$i_{Lr}(t) = -\frac{V_{FW}}{L_r}t + I_{\min} + \frac{V_o}{Z_r} \quad (37)$$

$$-\frac{V_{FW}}{L_r}D_{\max}T + I_{\min} + \frac{V_o}{Z_r} > I_{\max} \quad (38)$$

$$I_{\max} = I_{\min} + \Delta i_L \quad (39)$$

$$-\frac{V_{FW}}{L_r}D_{\max}T + \frac{V_o}{Z_r} > \Delta i_L. \quad (40)$$

B. Resonant Inductor

In Fig. 6, the time of interval 2, which is the rising time of the resonant inductor current, is expressed by (41). For the maximum resonant current, the time of interval 3, which is the resonant time of the resonant inductor and capacitor, is defined as one-fourth of the resonant period. As a rule of thumb, the rising time of the resonant inductor current (intervals 2–3) can be set to 10% of the minimum on time. This is expressed as (43)

$$t_3 - t_2 = \frac{L_r}{V_o}I_{\min} \quad (41)$$

$$t_4 - t_3 = \frac{T_r}{4} \quad (42)$$

$$\frac{L_r}{V_o}I_{\min} + \frac{T_r}{4} = 0.1 D_{\min}T. \quad (43)$$

From (40) and (43), the resonant inductor is expressed as

$$L_r < \left(\frac{2}{\pi}D_{\min}TV_o - V_{FW}D_{\max}T \right) / \left(\Delta i_L + \frac{2}{\pi}I_{\min} \right). \quad (44)$$

C. Resonant Capacitor

The resonant capacitor is connected to the switch in parallel. Thus, the waveforms of the resonant capacitor voltage and switch voltage are equivalent at turn-off. To satisfy the ZVS condition, the resonant capacitor can be selected to exceed ten times the output capacitance of the switch. However, the capacitor is charged by the main inductor current and the resonant inductor current at turn-off. Thus, it can be selected to exceed twenty times the output capacitance of the switch. Equation (43) is simplified to

$$C_r = \frac{0.04D_{\min}^2T^2}{\pi^2L_r} + \frac{4I_{\min}^2L_r}{\pi^2V_o^2} - \frac{0.8I_{\min}D_{\min}T}{\pi^2V_o}. \quad (45)$$

The design of the resonant inductor and capacitor are based on (44) and (45).

V. SIMULATION RESULTS

This paper simulated the adopted soft-switching boost converter and the PV module modeling of 700 W using the PSIM software. Fig. 7 shows the simulated output characteristic waveform of the PV module, which controlled the MPPT using dynamic link libraries (DLLs) for the PSIM software. At 0.4 s, this converter starts estimating the maximum power point. After 0.925 s, the MPPT is completed. At this time, the simulated PV module reaches the maximum power of 700 W,

and then, the output voltage and current of simulated PV module are 194.3 V and 3.6 A, respectively. Fig. 8 shows the main inductor current and the pulsewidthmodulation (PWM) gate signal of the main switch. When the main switch is turned on, the energy of inductor is accumulated.

When it is turned off, this energy is transferred to the output. Fig. 9 shows the waveforms of the output diode voltage and the current. Fig. 10 shows the waveforms of the resonant capacitor voltage and the resonant inductor current. Fig. 11 shows the current and voltage waveforms of the switch. Via resonance of the resonant inductor and capacitor, ZVS and ZCS are achieved at turn-on and turn-off.

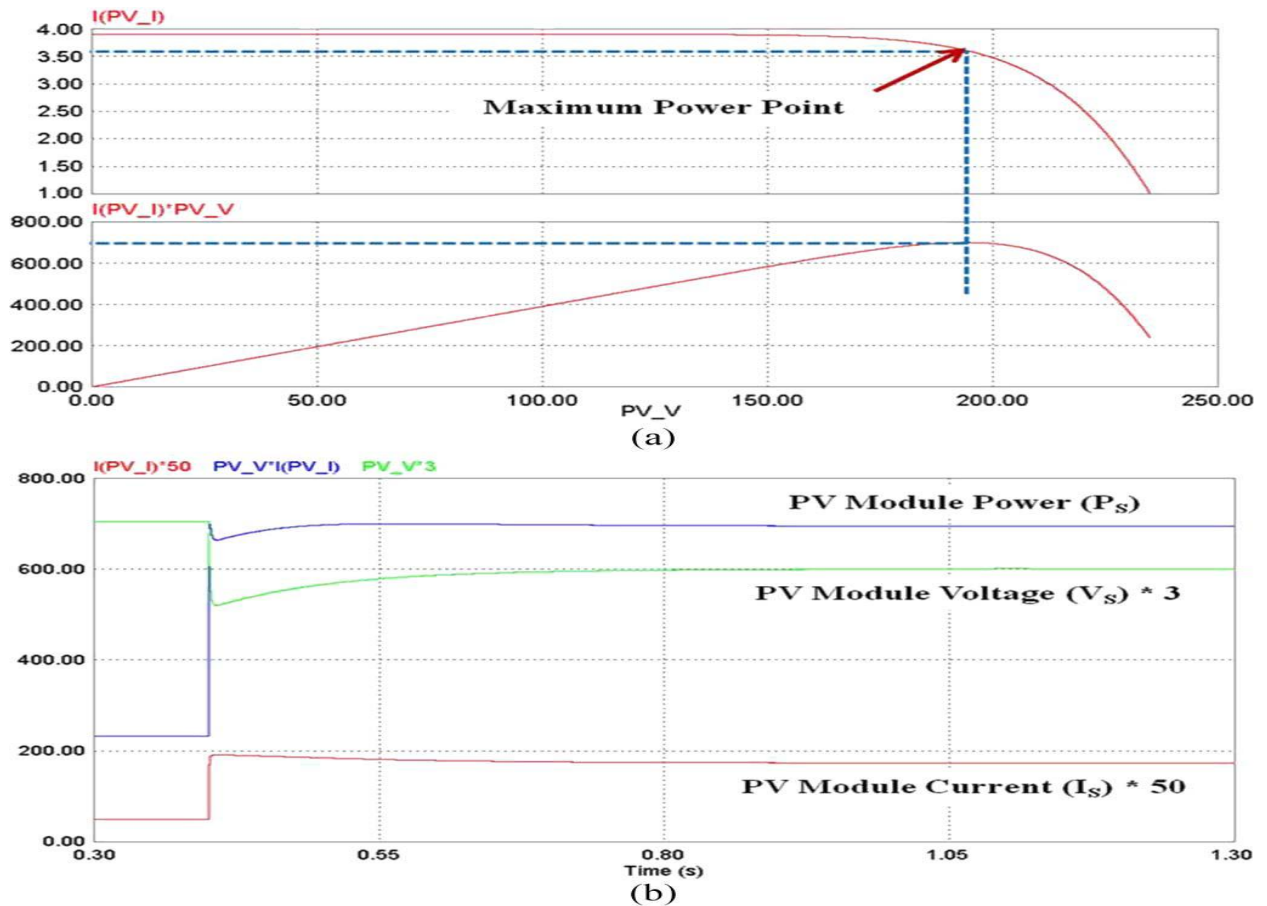


Fig. 7. Simulated output characteristic waveforms of PV module.
 (a) Simulated I - V and power curves of PV module. (b) Simulated real-time waveforms of power, voltage, and current.

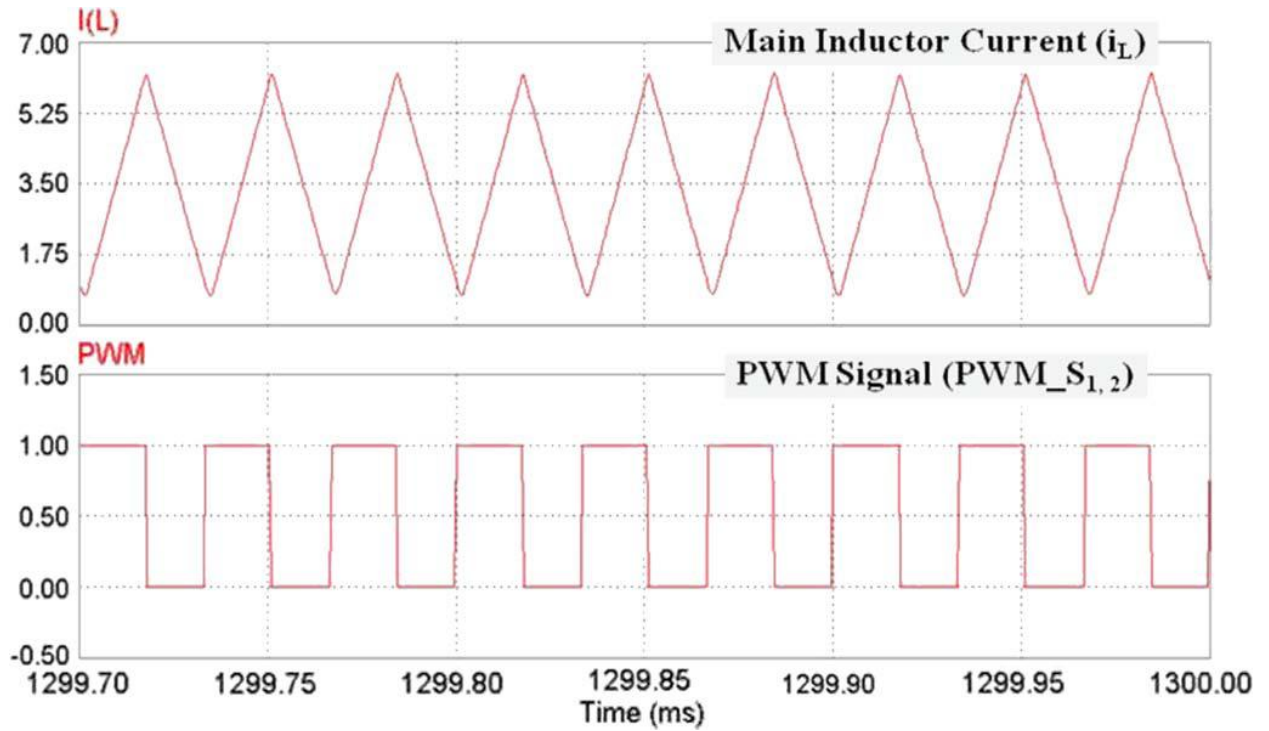


Fig. 8. Simulated waveforms of the gate signal and the main inductor current.

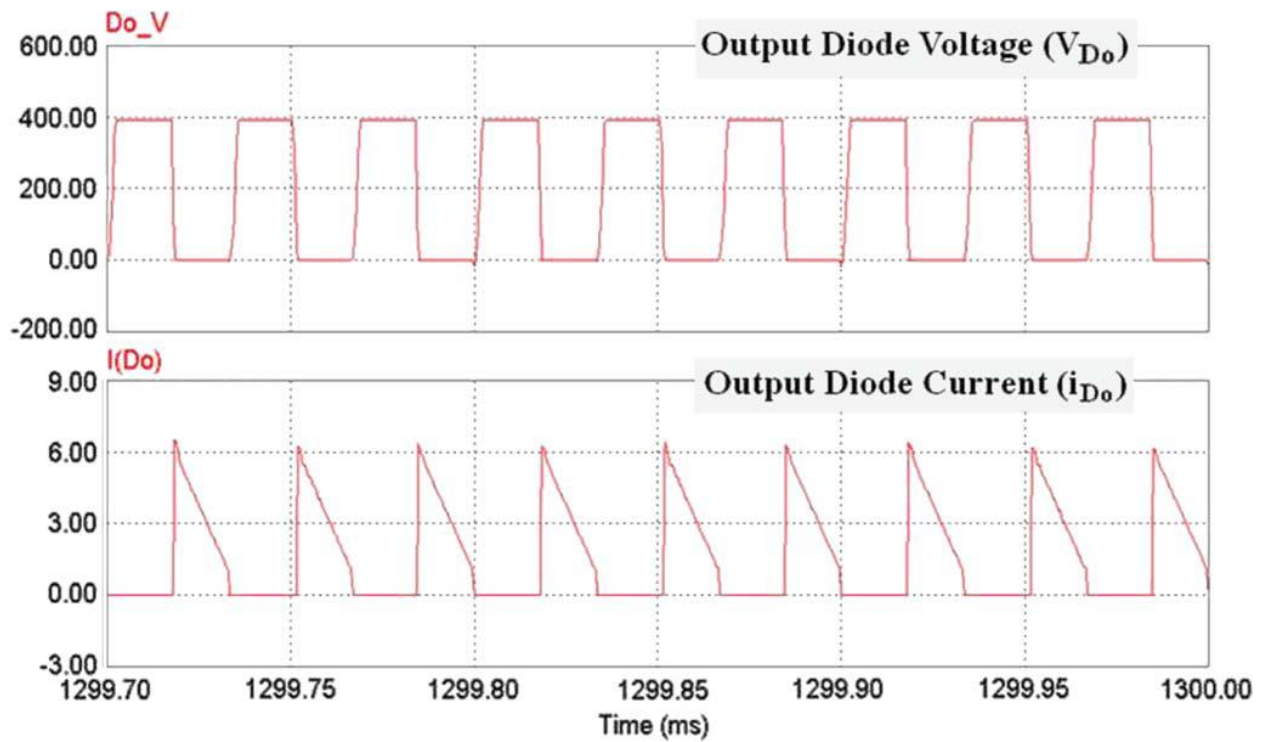


Fig. 9. Simulated waveforms of the output diode voltage and the current.

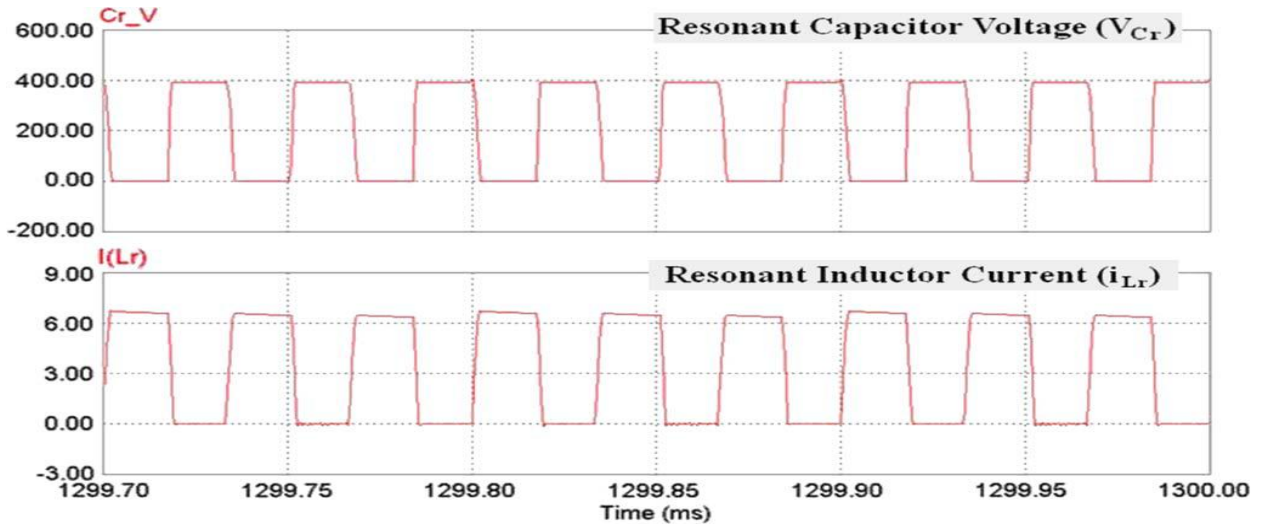


Fig. 10. Simulated waveforms of the resonant capacitor voltage and the resonant inductor current.

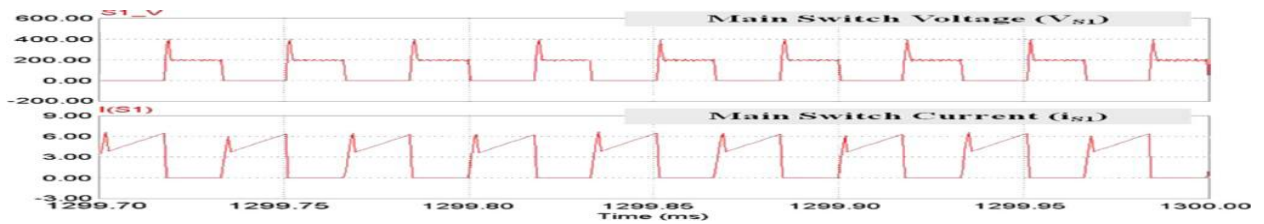


Fig. 11. Simulated waveforms of the main switch voltage and the current.



Fig. 12. Experimental setup using the Solarsim-10k PV simulator.

VI. EXPERIMENTAL RESULTS

The converter in this paper supplied the 700-W characteristic of a Solarsim-10K PV simulator. The output current and the voltage of a PV simulator were sensed and controlled by the P&O algorithm for the MPPT using an ATmega128. To confirm the aforementioned operations, the proposed soft-switching boost converter was experimented. Fig. 12 shows the experimental setup of specifications in Table I. In Fig. 12, the test bed to the left is the proposed converter, and the equipment in the center is the PV simulator Solarsim-10k. This PV simulator can be setting up the cell number, irradiance, and operating temperature. In this paper, the irradiance and operating temperature of the Solarsim-10k PV simulator were set as 0.9 kW/m² and 25 °C, respectively. Fig. 13 shows the $V-I$ and $V-P$ characteristic curve of the PV simulator used as the source of this converter. Oscillations at the edge of the characteristic curve are controlled by the maximum power point. Based on this waveform, the converter controlled the MPPT effectively.

TABLE I
CONVERTER SPECIFICATIONS AND IMPLEMENTATION DETAILS

Maximum Power	$P_{o,max}$	700[W]
Switching Frequency	f_s	30[kHz]
PV-Module Voltage	V_s	150–230[V]
Output Voltage	V_o	380[V]
Main Inductor	L	560[mH]
Resonant Induction	L_r	83[mH]
Resonant Capacitor	C_r	20[nF]
Output Capacitor	C_o	1000[μ F]
Main switch	S_1	FGA15N120
Auxiliary switch	S_2	FGA15N120
Auxiliary diodes	D_1, D_2	DSEI20-12A
Output diode	D_o	DSEI20-12A

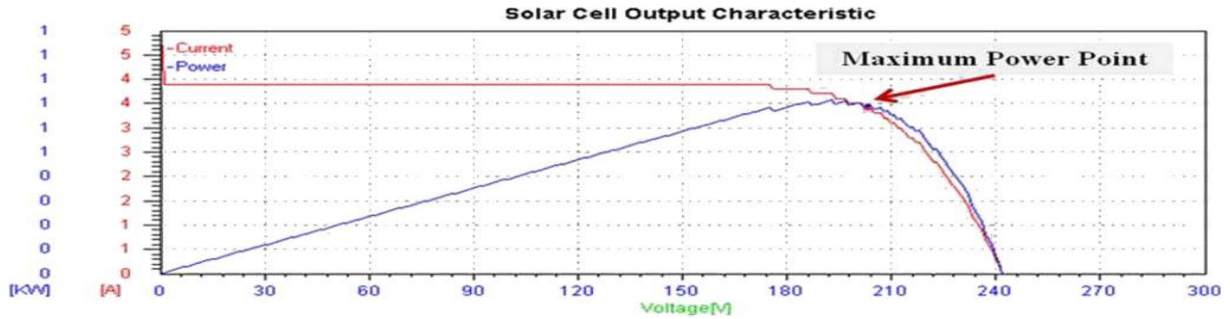


Fig. 13. Output characteristic curves of the PV simulator.
($V_s = 194.3$ V and $I_s = 3.6$ A at the maximum power point).

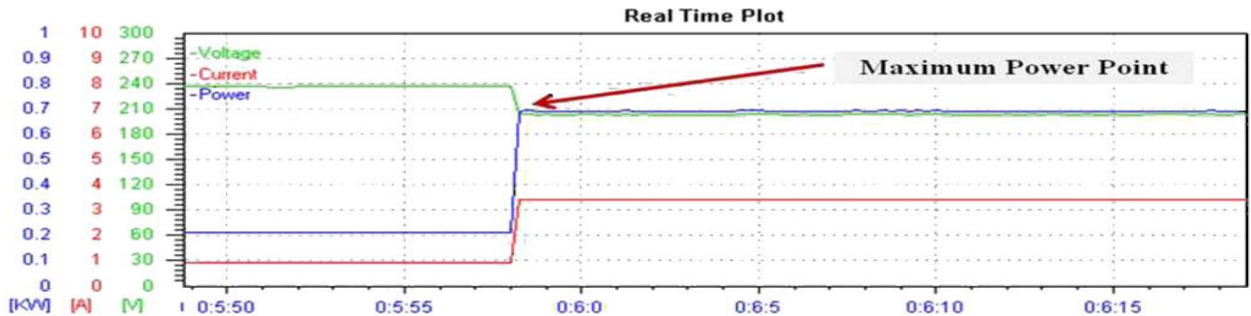


Fig. 14. Real-time voltage, current, and power waveforms of PV simulator.
($P_s = 700$ W, $V_s = 194.3$ V, and $I_s = 3.6$ A at the maximum power point).

Fig. 14 shows the current, voltage, and power with respect to time for the maximum power point. Based on this graph, the output voltage and current were 194.3 V and 3.6 A, respectively, and the output power reached 700 W at the maximum power point.

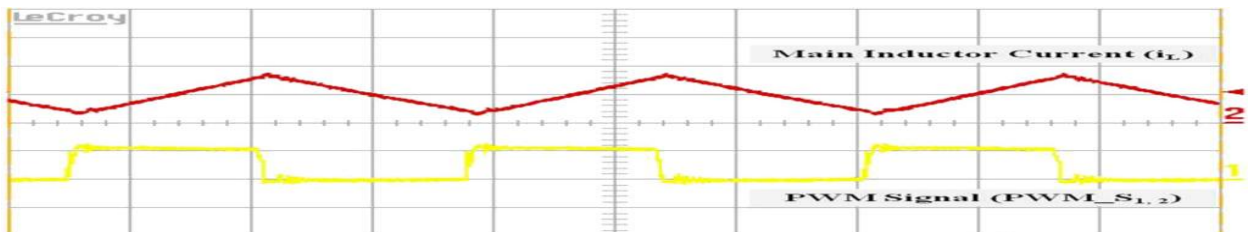


Fig. 15. Measured waveforms of the main inductor and the gate signal
(y-axis: $i_L = 4$ A/div and PWM_S1,2 = 10 V/div; x-axis: 10 μ s/div).



Fig. 16. Measured waveforms of the output diode voltage and current
(y-axis: $V_{Do} = 200$ V/div and $i_{Do} = 4$ A/div; x-axis: 10 μ s/div).

Fig. 15 shows the waveform of the main inductor current and the gate signal. By the PWM signal, the rising current of the main inductor at turn-on accumulates energy, and the decreasing current transfers the energy to the output of the converter.

Fig. 16 shows the current and the voltage waveform of the output diode. Based on this waveform, the diode is turned on under zero-current condition, and it is turned off under zero voltage condition. Thus, the switching losses of the diode can be reduced.

Fig. 17 shows the resonant inductor current, the resonant capacitor voltage, and the load voltage. When charging and discharging the capacitor, it is in resonance with the resonant inductor.

Fig. 18 shows the switch current and voltage wave forms, when the switch is turned on under zero-current condition by the resonant inductor and it is turned off under zero-voltage condition by the resonant capacitor.

Fig. 19 shows the efficiency of the proposed converter. As shown, the efficiency of the proposed converter is improved by about 4%. In this paper, the efficiency is measured as follows. The power supply (KJP-18K) is connected to the input of the converter, and the electric load (EL-3000P) is connected to the output. Moreover, the converter is tested by varying the load.

The efficiency is measured by the power analyzer PM 3000A. We compared the conventional hard-switching converter and the adopted converter under the same switching frequency and power conditions.

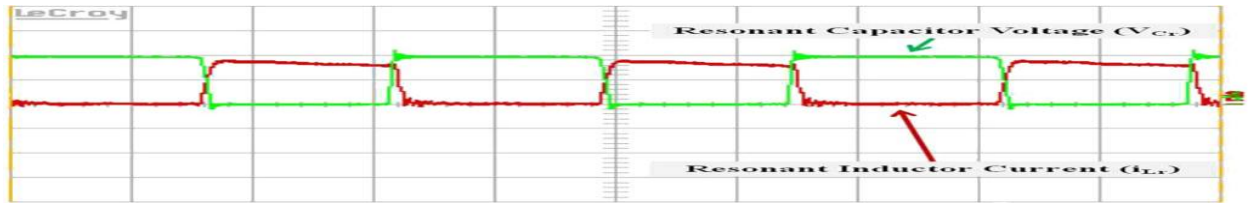


Fig. 17. Measured waveforms of the resonant inductor current and resonant capacitor voltage (y-axis: $V_{Cr} = 200$ V/div and $i_{Lr} = 4$ A/div; x-axis: $10 \mu\text{s}/\text{div}$).



Fig. 18. Measured waveforms of the main switch voltage and current (y-axis: $V_{S1} = 200$ V/div and $i_{S1} = 4$ A/div; x-axis: $10 \mu\text{s}/\text{div}$).

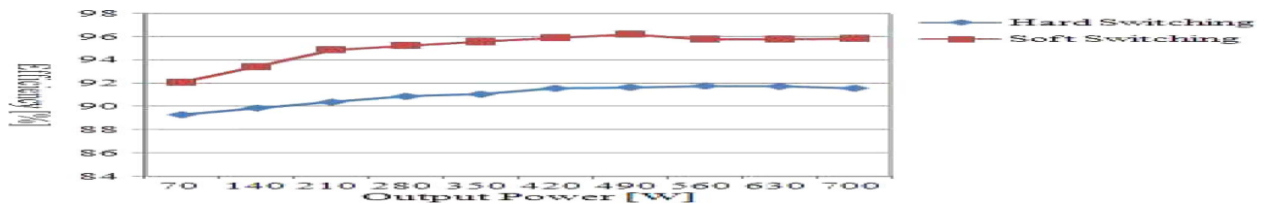


Fig. 19. Efficiency under the entire load conditions.

VII. CONCLUSION

In this paper, we proposed a soft-switching boost converter, which involved an added SARC in the conventional boost converter. This soft-switching boost converter is easy to control because the two switches are controlled by the same PWM signal. All of the switching devices in this converter achieved ZCS and ZVS by the resonant inductor and capacitor at turn/off. Therefore, the switching losses were reduced dramatically. This paper has analyzed the operational principles of the adopted converter and applied them to the P&O algorithm, which is a kind of MPPT method. Moreover, this converter was verified by the simulation and experimental results. This soft-switching boost converter can be applied to a stand-alone and a grid-connected system using a PV power conditioning system.

REFERENCES

- [1]. R. Gules, J. De Pellegrin Pacheco, H. L. Hey, and J. Rnhoff, "A maximum power point tracking system with parallel connection for PV stand alone applications," *IEEE Trans. Ind. Electron.*, vol. 55, no. 7, pp. 2674–2683, Jul. 2008.
- [2]. F. Liu, S. Duan, F. Liu, and Y. Kang, "A variable step size INC MPPT method for PV system," *IEEE Trans. Ind. Electron.*, vol. 55, no. 7, pp. 2622–2628, Jul. 2008.
- [3]. H. Bodur and A. Faruk Bakan, "A new ZCT-ZVT-PWM DC–DC converter," *IEEE Trans. Power Electron.*, vol. 19, no. 3, pp. 676–684, May 2004.
- [4]. J.-H. Kim, D.-Y. Yung, S.-H. Park, C.-Y. Won, Y.-C. Jung, and S.-W. Lee, "High efficiency soft-switching boost converter using a single switch," *J. Power Electron.*, vol. 9, no. 6, pp. 929–939, Nov. 2009.

- [5]. J.-P. Lee, B.-D. Min, T.-J. Kim, D.-W. Yoo, and J.-Y. Yoo, "Design and control of novel topology for photovoltaic dc/dc converter with high efficiency under wide load ranges," *J. Power Electron.*, vol. 9, no. 2, pp. 300–307, Mar. 2009.
- [6]. J.-J. Lee, J.-M. Kwon, E.-H. Kim, and B.-H. Kwon, "Dual series resonant active clamp converter," *IEEE Trans. Ind. Electron.*, vol. 55, no. 2, pp. 699–710, Feb. 2008.
- [7]. X. Wu, J. Zhang, X. Ye, and Z. Qian, "Analysis and derivations for a family ZVS converter based on a new active clamp ZVS cell," *IEEE Trans. Ind. Electron.*, vol. 55, no. 2, pp. 773–781, Feb. 2008.
- [8]. S.-S. Lee and G.-W. Moon, "Full ZVS range transient current buildup half bridge converter with different ZVS operations to load variation," *IEEE Trans. Ind. Electron.*, vol. 55, no. 6, pp. 2557–2559, Jun. 2008.
- [9]. M. Z. Youssef and P. K. Jain, "Series parallel resonant converter in self sustained oscillation mode with the high frequency transformer leakage inductance effect: Analysis, modeling, and design," *IEEE Trans. Ind. Electron.*, vol. 54, no. 3, pp. 1329–1341, Jun. 2007.
- [10]. R. Casanueva, F. J. Azcondo, and C. Branas, "Output current sensitivity analysis of the LCpCs resonant inverter: Current source design criteria," *IEEE Trans. Ind. Electron.*, vol. 54, no. 3, pp. 1560–1568, Jun. 2007.
- [11]. S. Zheng and D. Czarkowski, "Modeling and digital control of a phase controlled series parallel resonant converter," *IEEE Trans. Ind. Electron.*, vol. 54, no. 2, pp. 707–715, Apr. 2007.
- [12]. D. J. Tschirhart and P. K. Jain, "A CLL resonant asymmetrical pulse width modulated converter with improved efficiency," *IEEE Trans. Ind. Electron.*, vol. 55, no. 1, pp. 114–122, Jan. 2008.
- [13]. N. D. Benavides and P. L. Chapman, "Modeling the effect of voltage ripple on the power output of photovoltaic modules," *IEEE Trans. Ind. Electron.*, vol. 55, no. 7, pp. 2638–2643, Jul. 2008.
- [14]. G.-R. Cha, S.-H. Park, C.-Y. Won, Y.-C. Jung, and S.-H. Song, "High efficiency soft switching boost converter for photovoltaic system," in *Proc. 13th EPE-PEMC*, Sep. 1–3, 2008, pp. 383–397.
- [15]. Y. C. Jung, J. G. Cho, and G. H. Cho, "A new zero voltage switching resonant DC-link inverter with low voltage," in *Proc. IEEE IECON*, Oct. 28–Nov. 1 1991, vol. 1, pp. 308–313.